White Rose
university consortium
Universities of Leeds, Sheffield & York

Improving models of pedestrian crossing behavior using neural signatures of decision-making

Siwei Ma[1], Xuedong Yan[1*], Jac Billington[2], Matteo Leonetti[3], Natasha Merat[4], Gustav Markkula[4]

1 MOT Key Laboratory of Transport Industry of Big Data Application Technologies for Comprehensive Transport, Beijing Jiaotong University, Beijing 100044, PR China.

2 School of Psychology, University of Leeds, Leeds LS2 9JT, U.K.

3 Department of Informatics, King's College London, London, UK

4 Institute for Transport Studies, University of Leeds, Leeds LS2 9JT, U.K.

∗ Corresponding author.

E-mail addresses: 22110287@bjtu.edu.cn (S. Ma), xdyan@bjtu.edu.cn (X. Yan), j.billington@leeds.ac.uk (J. Billington), matteo.leonetti@kcl.ac.uk (M. Leonetti), n.merat@its.leeds.ac.uk (N. Merat), g.markkula@leeds.ac.uk (G. Markkula)

Abstract: Understanding and modelling pedestrian behavior is important for traffic safety, not least in the context of vehicle automation. There exist competing models for how pedestrians decide if and when to cross a road with oncoming traffic. Distinguishing between these competing models is non-trivial, but recent results in the cognitive neuroscience of decision-making offer a promising method, complementing behavioral data with electroencephalography (EEG): Previous EEG studies have shown that the centro-parietal positive potential (CPP) reflects evidence accumulation during abstract perceptual decision-making tasks, and that it can be used to arbitrate between alternative models of these tasks. However, it is not yet known whether the CPP can be used to support modeling in more complex, embodied contexts, such as human locomotion in road traffic. Here, we address this question by designing an EEG paradigm for pedestrian road-crossing. In a computer-based experiment, participants made road-crossing decisions in a simulated scenario where a car approached them under different time-to-arrival (TTA) conditions. Three perception-based drift diffusion models and one utility-based drift diffusion model were used to model the pedestrian behavior. The behavioral data showed a partial preference for the utility-based model over the perception-based drift diffusion models. The EEG data showed a CPP signal, which helped distinguish between the models in a way that behavioral data alone could not: CPP amplitude was positively correlated with accumulated evidence in the drift-diffusion models, and with stronger correlations for the utility-based model than for the perception-based models. Our results show that the CPP signature can be used to help arbitrate between competing decision-making models also in more embodied tasks, a finding which has applied implications not least in the context of traffic safety engineering and vehicle automation.

1 Introduction

Decision-making is a critical cognitive process that underlies human behavior in various contexts, not least in human locomotion and interaction in road traffic (González-Méndez et al., 2021; Wang et al., 2024). Autonomous vehicles (AVs) face great challenges in interacting with pedestrians, prompting researchers to focus on modeling pedestrian behavior to better predict their road-crossing decisions. Competing models have been proposed to explain how pedestrians decide if and when to cross roads with oncoming traffic. It is crucial to identify models that achieve high prediction accuracy, and which ideally also accurately replicate human decision-making processes, to maximize generalization performance. These models are pivotal for designing AV systems capable of anticipating and responding effectively to pedestrian behavior, thereby enhancing safety and facilitating the seamless integration of AVs into transportation networks (Camara et al., 2020; Markkula et al., 2020).

The decision-making process can be captured from a behavioral modeling perspective. Several evidence accumulation models have been proposed, including the drift-diffusion model (DDM; Ratcliff, 1978), Ornstein–Uhlenbeck model (Busemeyer & Townsend, 1993), and the Linear Ballistic Accumulator (Brown & Heathcote, 2008). These models translate accuracy and response time into psychologically interpretable constructs assumed to underlie decision-making processes (Bogacz et al., 2006; Parker and Ramsey, 2024). Here, we focus on the DDM, which serves as a foundational model bridging cognitive theories and computational modeling for understanding the decision-making process. Proposed by Ratcliff (1978), the DDM offers a principled framework for comprehending decision-making mechanisms in two-choice tasks, effectively capturing both the choices made and the corresponding decision times (Ratcliff & McKoon, 2008; Nunez et al., 2017). The basic DDM includes four key parameters (Ratcliff, 1978): a drift rate representing evidence accumulation speed, a decision boundary representing the evidence threshold for decision-making, a starting position representing initial bias towards one option, and a non-decision time representing perception and motor execution delays external to the decision-making process. Since its development, researchers have extended the four-parameter DDM to the seven-parameter full DDM to account for inter-trial variabilities of the drift rate, non-decision time, and starting point bias (Ratcliff and Rouder, 1998; Ratcliff and Tuerlinckx, 2002).

Characterizing the state of mind solely through behavioral data is challenging because decision-making is fundamentally a process rooted in brain activity (Turner et al., 2015). Within neuropsychological research, there has been a growing interest in studying how the neural processes underlying evidence accumulation contribute to decision-making (Forstmann et al., 2010; Steinemann et al., 2018; Yau et al., 2021). This interest has led to a focus on event-related potential (ERP) components such as the centro-parietal positivity (CPP), which is thought to reflect how the brain processes and

integrates information in the lead up to a decision (O'Connell et al., 2012; Kelly & O'Connell, 2013; Kohl et al., 2020). CPP has been analyzed in simple perceptual decision-making tasks and tasks requiring response selection based on probabilistic information. For example, studies have utilized CPP in tasks involving random dot-motion perception (Kelly and O'Connell, 2013; Kohl et al., 2020), gradual contrast-change detection (O'Connell et al., 2012; McGovern et al., 2018), and face recognition (Van Vugt et al., 2019). In all of these tasks, CPP shows a peak at the time of response. However, it is not known whether the CPP signature is present in more embodied decision-making tasks, such as locomotor tasks, where one decides about one's own movement in the world.

Combining neural data with mathematical modeling - commonly referred to as model-based cognitive neuroscience - can provide a better understanding of the decision-making process (Forstmann et al., 2011; Forstmann & Wagenmakers, 2014; Turner et al., 2015). Most studies of model-based cognitive neuroscience have utilized a two-stage correlational procedure: First, the model is fitted to behavioral data to generate the best-fitting parameters, and neural signatures are extracted from the raw neural data. Then, correlations are analyzed to test whether the underlying processes assumed by the cognitive model are reflected in the brain (Forstmann et al., 2008; Purcell et al., 2010; Turner et al., 2015). This type of combination of DDM modelling with CPP observations has previously proven fruitful. For example, in a face-morphing decision-making task, Yau et al. (2021) identified a covariation between CPP amplitude, and the drift rate parameter derived from the DDM. In another study, utilizing both perception- and memory-based face stimuli (Van Vugt et al., 2019), participants were required to determine whether two faces shown at different angles represented the same person (the perception task) and whether a test face matched previously shown faces (the memory task). Van Vugt et al. (2019) observed that the CPP slope was related to the drift rate parameter for both tasks. These findings demonstrated the possibility of using DDM to represent the actual decision-making process in the brain (as indicated by CPP) across different lab-based tasks. However, it is unclear whether this type of connection between mathematical decision-making models and brain activity can be established in more complex behaviors like driving a vehicle or walking and interacting with traffic.

Recently, there have been several attempts to model decision-making using the DDM in applied road traffic scenarios, such as drivers' left-turn gap acceptance (Zgonnikov et al., 2024) and pedestrians' road-crossing behavior (Lin et al., 2022; Pekkanen et al., 2022; Theisen et al., 2024). There are two kinds of models based on different theoretical frameworks in DDM modeling, which can be referred to as perception-based versus utility-based models. Perception-based models derive the evidence to be accumulated directly from perceptual heuristics (Pekkanen et al., 2022; Zgonnikov et al., 2024; Theisen et al., 2024), whereas utility-based models provide derive the evidence from the estimated future utility of the action being decided upon (Lin et al., 2022; Markkula et al., 2023; for related approaches in non-

traffic contexts see also Drugowitsch et al., 2012; Tajima et al., 2016). There is currently a lack of direct comparison between these two types of models.

The aforementioned studies highlight the effectiveness of the DDM modelling framework in describing human decision-making in the road traffic context. However, none of them have included an analysis of neural characteristics. Only one study, on collision threat detection, has analyzed CPP and DDM simultaneously, demonstrating that a DDM could predict the onset of the CPP signature (Markkula et al., 2021), but this study focused purely on perception, excluding any decision-making regarding one's own movement, and did not measure the correlation between CPP and DDM evidence.

Based on the research gaps outlined above, the aim of the present study was to compare perception-based and utility-based models of pedestrian road crossing, and whether CPP analyses could be used to further support such a comparison. Since both CPP and DDM describe the process of evidence accumulation in decision-making - CPP reflecting this process in the brain and DDM simulating it within computational models - there may be a correlation between the two. A higher correlation would suggest that the evidence accumulation process in DDM closely mirrors that in the brain, as reflected in CPP. To this end, a computer-based pedestrian crossing experiment was conducted, where participants were instructed to initiate road crossings at a time of their choice by pressing a button, and their electroencephalography (EEG) and behavioral responses were recorded simultaneously. The CPP signal was extracted, and behavioral data were modeled using the different DDM variants. The correlation between CPP amplitude and accumulated evidence in DDM was examined to illustrate the cognitive evidence accumulation process underlying decision-making in the road-crossing task.
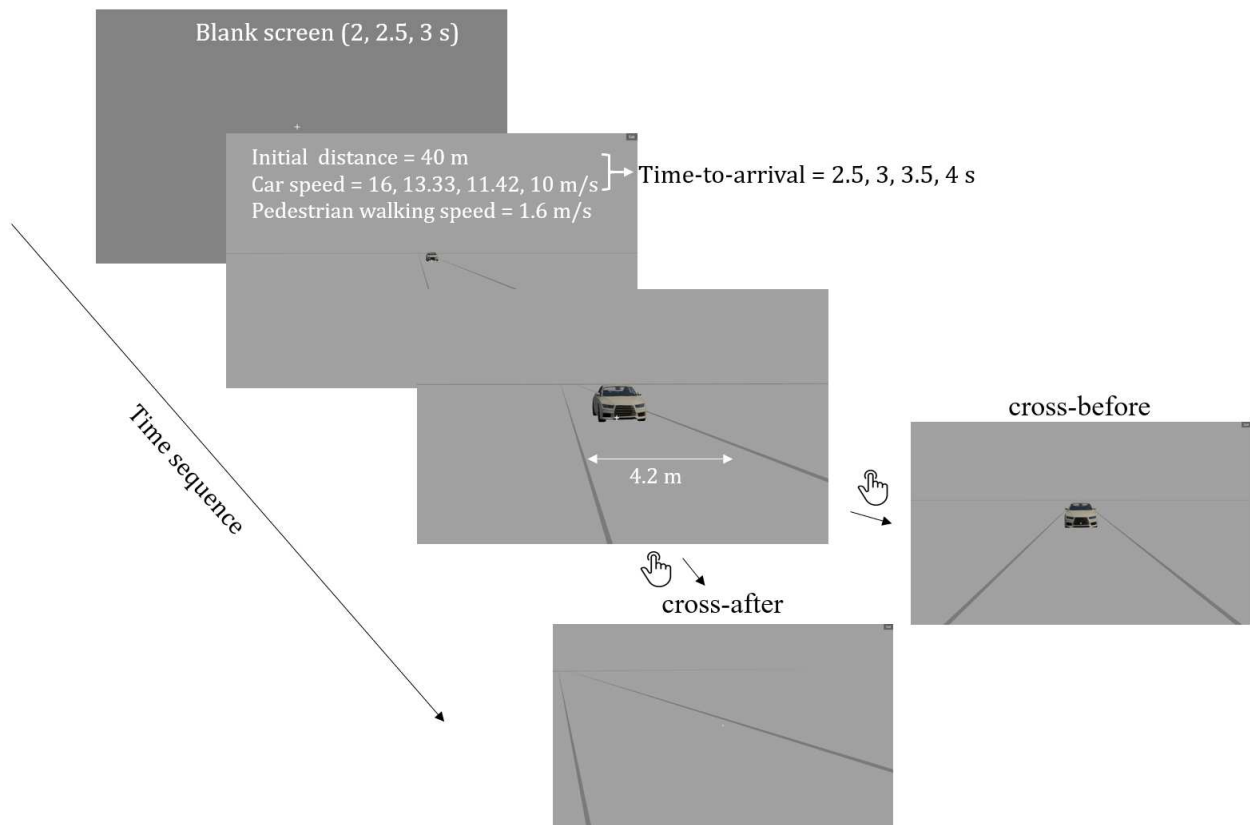
2 Method

2.1 Participants and apparatus

Sixteen right-handed participants (9 males, 7 females; mean age 31 years, range 26–42) completed the experiment, recruited via the subject pool of the School of Psychology, University of Leeds. The sample size was determined based on previous studies analyzing CPP (e.g., n=9 in Forstmann et al., 2010; n=13 in Kelly and O'Connell, 2013; n=19 in Kelly et al., 2019). All participants had normal or corrected-to-normal vision, and no history of psychiatric diagnosis or severe brain injury. The experiment took approximately 90 minutes, and each participant provided informed consent before participating and was compensated with a gift voucher worth £20 after completing the experiment. The study was approved by the School of Psychology Research Ethics Committee at the University of Leeds (Reference: PSYC-266).

In this computer-based experiment, we utilized Unity® for creating high-quality 3D scenes and motion control. Behavioral responses were recorded at the 60 Hz refresh rate of the screen. Meanwhile, participants' EEG data were recorded using a Biosemi ActiveTwo system with a 64-channel 10–20
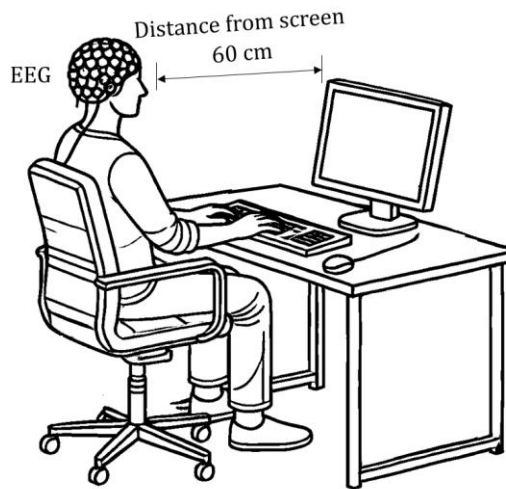
international cap and six additional electrodes, including four channels for electrooculogram (EOG) to monitor lateral and dorsal eye movements, along with two mastoid electrodes. The data were recorded at a 1,024 Hz sampling rate and then downsampled to 256 Hz immediately after acquisition using ActiTools software (version 9.01).

2.2 Experimental design

The experiment was designed as a within-subjects repeated measures study with four time-to-arrival (TTA) conditions. **Figure 1** depicts one experimental trial and the schematic of experiment setup. Each trial began with an auditory chime followed by the presentation of a fixation cross on a grey background, which lasted 2 s, 2.5 s, or 3 s, selected at random. Then the stimulus car image appeared centrally on the screen, signaling the start of the pedestrian crossing scenario. The participant's point of view (the "camera" in the virtual environment) was consistently directed toward the geometrical center of the car to simulate a realistic crossing view. In each trial, the initial distance between the car and the pedestrian was fixed at 40 m. The car approached the participant's crossing location at speeds of 16 m/s, 13.33 m/s, 11.42 m/s, and 10 m/s, corresponding to four TTA conditions (2.5 s, 3 s, 3.5 s, and 4 s). These vehicle speeds, ranging from 36 km/h to 57.6 km/h, are typical in urban traffic environments where vehicles frequently interact with pedestrians. There was also a small per-trial jitter of ±0.1 s, to minimize the risk of the four discrete trial types becoming individually recognizable to participants. The car approached participants from either the left or right side, with equal frequency. There were no audio cues when the car was approaching, to avoid the influence of auditory information on participant judgments (Schiff & Oldak, 1990). The road width was 4.2 m, and the participant's initial position was 0.5 m from the roadside. Once the participant decided to cross, they were required to press the forward slash key on a computer keyboard, at which point the participant's location in the virtual world was translated across the road, emulating a road crossing. Participants could choose freely when to cross, i.e. typically either before the car passed or after the car had passed. In this paper, we will refer to these decisions as cross-before and cross-after. The pedestrian's walking speed was maintained at 1.6 m/s, which is considered a typical fast walking speed (Fitzpatrick et al., 2006). If there was a collision between the participant and the car, the participant would hear a warning beep at the time of collision. After completion of a crossing, the scene faded out for 0.25 s before initiating a new trial.

Blank screen (2, 2.5, 3 s)

Initial distance = 40 m
Car speed = 16, 13.33, 11.42, 10 m/s ⎤ Time-to-arrival = 2.5, 3, 3.5, 4 s
Pedestrian walking speed = 1.6 m/s ⎦

Time sequence

4.2 m

cross-before

cross-after

(a)

Distance from screen
60 cm

EEG

(b)

Fig. 1 (a) Example of one trial of the pedestrian crossing experiment, and (b) Schematic of the task setup.

2.3 Procedure

Participants were required to sit at approximately 60 cm distance from the screen in a darkened EEG laboratory. The experiment began with a 5-minute practice block consisting of 16 trials. After the practice, participants proceeded to conduct the formal testing on their own. The formal testing consisted of 4 experimental blocks, with each block including 64 trials (4 TTAs × 2 Directions × 8 Repetitions), resulting in a total of 256 trials. The trial order was fully randomized within each block and across all participants.

Participants were allowed to take self-paced breaks between blocks. During the experimental blocks, they were instructed to maintain their gaze on the fixation target, refrain from blinking while the car was displayed and until their response.

2.4 Data preprocessing

EEG preprocessing was done using EEGLAB 2019 (Delorme & Makeig, 2004) and Fieldtrip (Oostenveld et al., 2011). The main steps of preprocessing were in line with Boyle et al. (2022), as follows:

All data were checked by eye, and channels exhibiting obvious poor quality were removed. The continuous data were then re-referenced to the average of all 64 channels. The data were high-pass filtered using a finite impulse response (FIR) filter with separate cut-offs of 1 Hz and 0.1 Hz. Subsequently, both sets of filtered data underwent a low-pass filter with a 40 Hz cut-off. Independent component analysis (ICA; Delorme et al., 2007) was used to decompose components from the 1 Hz filtered dataset and the derived ICA components were then removed from the 0.1 Hz filtered set to remove artefacts. This procedure preserves the integrity of ERP components by preventing the distortion that can occur when applying ICA to EEG data filtered at 0.1 Hz (Boyle et al., 2022). A baseline correction was applied using the 200 ms period before the car appeared. Data were then segmented into epochs of 1 s as follows: Stimulus-locked epochs, [-0.1, 0.9] s around the time of car appearance, and response-locked epochs, [-0.9, 0.1] s around the time at which the participant initiated a crossing. After defining the epochs, a MATLAB implementation of the Fully Automated Statistical Thresholding for EEG Artefact Rejection (FASTER; Nolan et al., 2010) was employed to identify and remove bad epochs from the data. Next, the five channels centered on Pz (CPz, POz, P1, P2) were averaged to yield the CPP amplitude, as in (Markkula et al., 2021).

2.5 Statistical analysis

To examine the effect of TTA conditions on CPP amplitude, we performed a multivariate F-test obtained from a Monte Carlo simulation with 1000 iterations in Fieldtrip. This test compared the CPP amplitude across each TTA condition at each time point in the stimulus-locked data and the response-locked data, including Bonferroni correction to control the overall Type I error rate (false positive). To test the difference in centro-parietal signal amplitude between cross-before and cross-after decisions, a similar Monte Carlo simulation was carried out using a T-test. These methods have been used in previous studies (Van Vugt et al., 2019; Boyle et al., 2022).

Pearson correlation analysis was done to analyze the relationship between CPP amplitude and the accumulated evidence in drift-diffusion models.

2.6 Evidence accumulation models

The evidence accumulation models constructed in this study were based on previous research, where TTA conditions were considered a primary variable influencing road-crossing decisions (Lin et al., 2022;

1   Pekkanen et al., 2022; Markkula et al., 2023; Zgonnikov et al., 2024). To verify this notion, logistic

2   regression analysis was conducted, demonstrating a significant influence of TTA conditions on decisions

3   of whether to cross before or after (B = 2.41, p < 0.01). The probability of cross-before decision for all

4   trials and response time for cross-before trials were shown in **Fig. 2**. As expected (Petzoldt, 2014; Tian et

5   al., 2022), a higher TTA was associated with a higher probability of a cross-before decision. Additionally,

6   the effect of TTA conditions on response time for cross-before decisions was found to be significant, with

7   response time increasing as TTA increased (F (3, 2240) = 48.20, p < 0.01). These statistical results are in

8   line with the model assumption that pedestrian's decisions are influenced by TTA conditions.
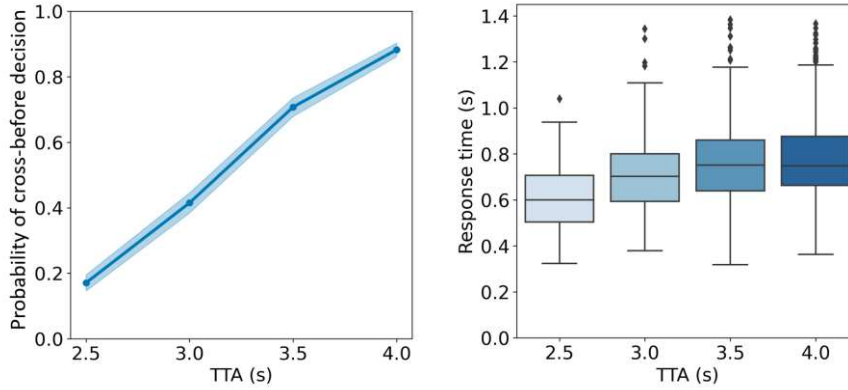
9

10   Fig. 2 The probability of a cross-before decision for all trials (left; shaded area represents 95% confidence interval) and

11   response time for cross-before trials (right).

12

13   Both perception-based and utility-based models were tested, with the former assuming that evidence

14   accumulation rates are obtained from heuristics applied to information that is perceptually available in

15   the scenario, especially TTA, and the latter assuming that evidence accumulation rates are obtained from

16   the perceived utility of crossing the road, at each point in time. These models represent different aspects

17   of the decision-making process. All models were implemented in PyDDM (Shinn et al., 2020).

18   2.6.1 Perception-based models

19   The perception-based models in this study were modified from the model proposed by Zgonnikov

20   et al. (2024), including the dynamic drift rate collapsing bound model (DC), dynamic drift rate fixed

21   bound model (DF) and static drift rate fixed bound (SF) model.

22   The definition of ***dynamic drift rate*** dx_d is shown in Eq. (1):

23

24     $$dx_d = \alpha \left(TTA_0 - t - \theta_{crit} \right) dt + dW \qquad (1)$$

25

26   Where α ($\alpha > 0$) quantifies the relative contribution of incoming perceptual information to the

27   accumulated evidence. θ_{crit} is a critical TTA threshold where the evidence accumulation begins only if

28   TTA is higher than θ_{crit}. *W* represents noise following a stochastic Wiener process (Ricciardi, 1976). The

dynamic drift rate assumes that the drift rate is influenced by the initial TTA conditions and that evidence stops accumulating towards the crossing boundary if the TTA at time t is lower than the critical threshold.

The **static drift rate** dx_s is defined similarly to the dynamic drift rate but without time dependency, as shown in Eq. (2). It assumes that the drift rate is influenced by the initial TTA conditions and the critical TTA threshold, and does not change over time.

$$dx_s = \alpha\left(TTA_0 - \theta_{crit}\right)dt + dW \qquad (2)$$

The **collapsing boundary** indicates that a decision is reached more quickly as time goes by because there is only a limited amount of time allowed for making decisions. The definition of collapsing boundary is as follows:

$$b(t) = \pm b_0 \times \frac{1}{\left(1 + e^{-k\left(TTA_0 - t - \tau\right)}\right)} \qquad (3)$$

Where b_0 represents the boundary scale parameter, multiplied by a sigmoid function of TTA to establish a collapsing bound. Parameter k ($k > 0$) defines the sensitivity of boundary to TTA, and τ equals to the TTA value when the boundary is at its baseline value ($\pm 1/2 b_0$).

The definition of a **fixed boundary** can be considered a special case of a collapsing bound model where the boundary $b(t)$ remains constant at $\pm b_0$, without employing the sigmoidal modulation.

Furthermore, a normally distributed **non-decision time** t_{ND} is included in all models to represent time delays associated with sensory perception and motor execution, as follows:

$$t_{ND} \in N(\mu_{ND}, \sigma_{ND}) \qquad (4)$$

2.6.2 Utility-based model

In the utility-based model, the pedestrian's decision-making process is formulated in terms of the utility of crossing, rendering more explicit trade-off between the benefits of making progress one one's journey and the costs of collision risk (Lin et al., 2022; Markkula et al., 2023). The utility-based model in this paper is based on (Lin et al, 2022) and (Markkula, 2023), in a simplified form adapted to this study's scenario.

The definition of **utility-based drift rate** dx_u is as follows:

$$dx_u(t) = \int_t^\infty \tanh(U - C(t'))dt' - \int_{TTA_0}^\infty \tanh(U)dt' + dW = \int_t^{TTA_0} \tanh(U - C(t'))dt' + dW$$

$$C(t') = \begin{cases} k_c/(TTA_0 - t'), & t' \le TTA_0 \\ 0, & t' > TTA_0 \end{cases} \tag{5}$$

In this expression, the integrals represent the estimated future total utility of crossing at time t versus waiting until time TTA_0 and crossing thereafter. In both cases after initiating crossing there is a utility with rate U for making progress, but if crossing in front of the car there is also a cost with rate $C(t')$. This can be thought of as a discomfort cost, increasing rapidly as the car comes closer. k_c represents the degree to which the subject is concerned about the risk of being hit; a higher value indicates greater caution. The hyperbolic tangent (tanh) function acts as a squashing function such that at the time of car passing ($t = TTA_0$), the value of $C(t')$ approaches infinity, while $\tanh(U - C(t'))$ approaches -1, ensuring that the function remains integrable.

We included a collapsing bound also for the utility-based model, and will thus refer to it here as the utility-based model with a collapsing bound (UC). The definitions of collapsing bound and non-decision time are the same as those described for the perception-based model.

2.6.3 Loss function

A negative log likelihood loss function was employed for model fitting to quantify how well the model's predictions matched the observed data. This approach measures the probability of the observed data under the model, with lower values indicating a better model fit. For the cross-before decisions, response times were binned with a size of 0.005 s, consistent with the model fitting timestep. For the cross-after decisions, all response times were aggregated into a single bin since they were not safety-critical. That is, our models do not make predictions about evidence accumulation after the car has passed. For each trial, the model predicted the probability of a response occurring in each bin, and these probabilities were then compared with the observed data. The likelihood of the observed data under the model was computed as the product of these probabilities across all trials, from which the negative log likelihood was derived. Akaike Information Criterion (AIC) values were then calculated based on the negative log likelihood to assess model fit and complexity.

3 Results

3.1 Centro-parietal signal dynamics in pedestrian crossing decisions

Fig. 3 depicts single-trial plots of the centro-parietal signal amplitude, illustrating the temporal relationship between the centro-parietal signal and response time at the trial level. Only trials with cross-before decisions were plotted. The upper topographical maps show the stimulus-locked and response-locked brain activity, covering a period from 50 ms before to 50 ms after the onset of the stimulus and

1 response time, respectively. It is clear that the amplitude of the centro-parietal signal steadily increases
2 with incoming evidence and reaches a high value around the response time.
3
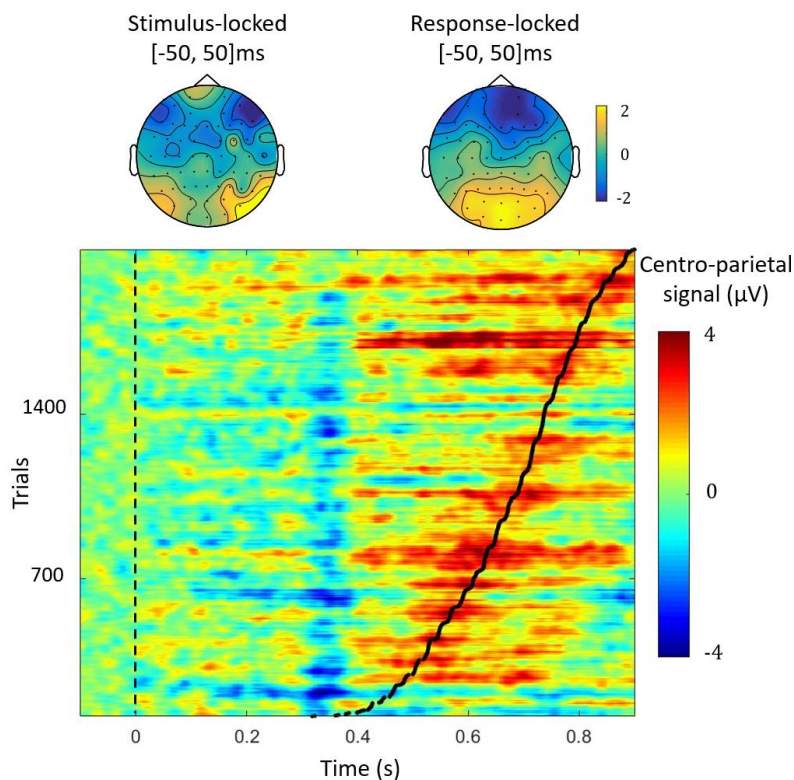
5 Fig. 3 Single-trial plots for temporal relation between the centro-parietal signal and response time (black line) for
6 cross-before decisions in all TTA conditions.

8 **Fig. 4** shows the stimulus-locked centro-parietal signal under different TTA conditions for cross-
9 before and cross-after decisions. The changes in centro-parietal signal amplitude for these two decisions
10 exhibit a similar pattern: Initially, there is a negative potential prior to the signal buildup at 300 – 350 ms,
11 which is likely influenced by visual evoked potentials triggered by a sudden stimulus onset, in our case
12 the car appearing on the screen. This observation is consistent with findings from other decision-making
13 tasks with a sudden appearance of a visual stimulus (Van Vugt et al., 2019). Subsequently, the signal
14 amplitude increases from around 350 ms in all conditions, representing the actual centro-parietal signal
15 positivity.
16 The comparison between different TTA conditions shows that for cross-before decisions, the buildup
17 of centro-parietal signal at a TTA of 2.5 s is significantly higher than the other TTA conditions, suggesting
18 that a TTA of 2.5 s elicits a more pronounced centro-parietal signal buildup in preparation for crossing
19 before the car. For cross-after decisions, the differences in centro-parietal signal buildup between different
20 TTA conditions was not statistically significant.
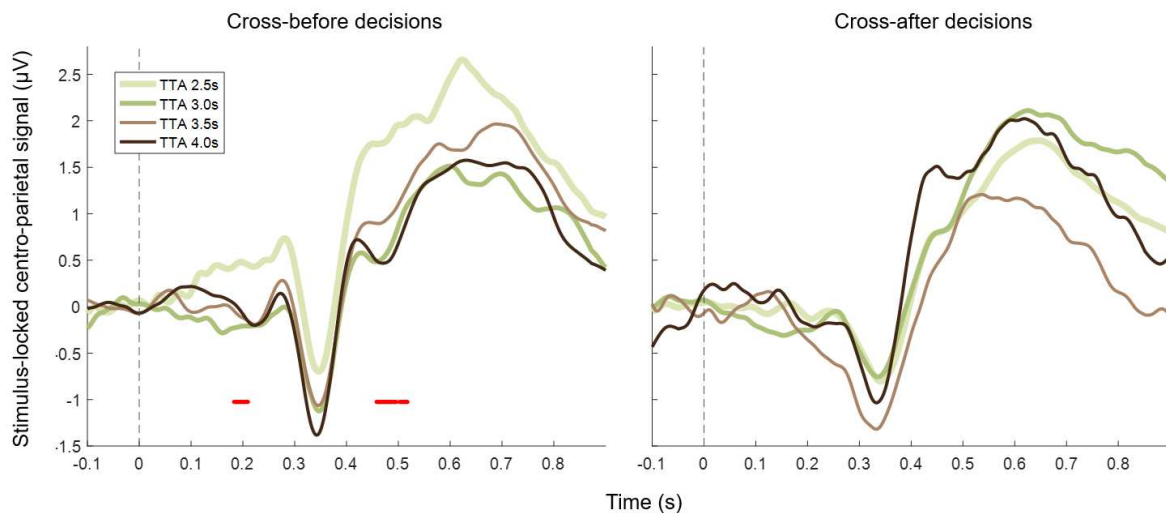
Fig. 4 Stimulus-locked centro-parietal signal of cross-before and cross-after decisions. Time 0 corresponds to car appearing time. Red dots indicate a significant difference in CPP amplitude between the four TTA conditions (Bonferroni corrected, $p < 0.05$). A moving average with 0.1 s window size was applied to smooth the data for visualization.

Fig. 5 shows the response-locked centro-parietal signal under different TTA conditions for cross-before and cross-after decisions. It's clear that the centro-parietal signal peaks at the time of response execution. This characteristic matches the feature of the CPP discussed in previous research (O'Connell et al., 2012; Kelly & O'Connell, 2013). Therefore, we refer to this signal as CPP from now on. The CPP at the response time for cross-before decisions shows a significant difference between the TTA conditions, with TTA values of 3.5 s and 4 s exhibiting higher values compared to TTA values of 2.5 s and 3 s. In contrast, there is no significant difference in response-locked CPP for cross-after decisions between different TTA conditions.

Looking between the cross-before and cross-after trials the CPP amplitude at the response time was higher for cross-before decisions than for cross-after decisions. A priori, it is not obvious whether one would expect a CPP peak at cross-after decisions, since it seems this decision is qualitatively different from the cross-before decision. Whereas the cross-before decision seems intuitively easy to understand as an evidence accumulation type of decision, the cross-after decision is arguably more of a timing task, where the participant simply waits until the car has passed and then presses the response key. Interestingly, our results suggest that also this type of task elicits a CPP peak.
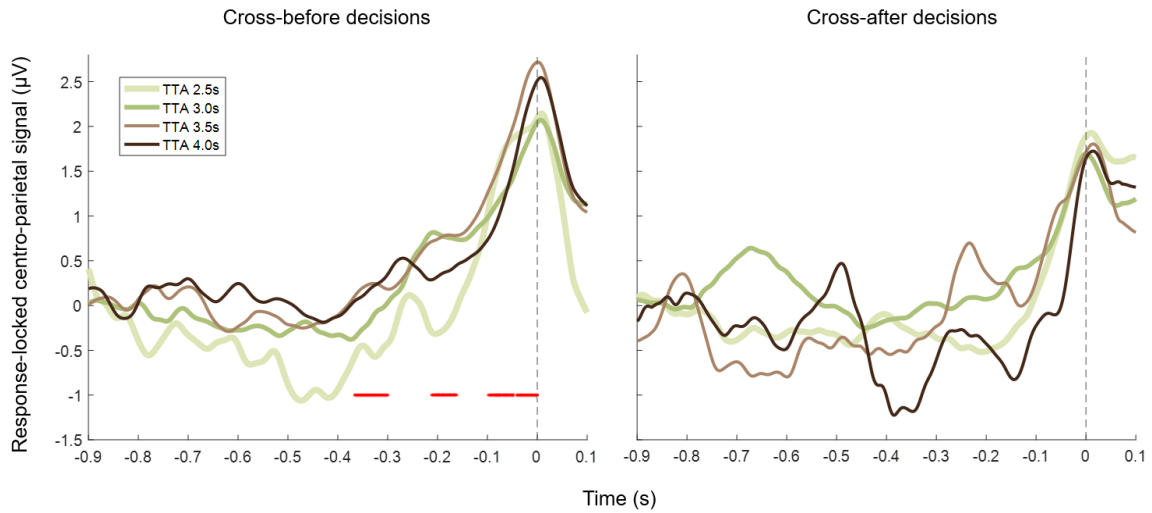
Fig. 5 Response-locked CPP of cross-before and cross-after decisions. Time 0 corresponds to response time. Red dots indicate a significant difference in CPP amplitude between the four TTA conditions (Bonferroni corrected, p < 0.05). A moving window of 0.1 seconds was used to smooth the data for visualization.

3.2 Fitting DDMs to pedestrian crossing decisions

AIC values were calculated for all participants to compare the four models, yielding the following results: UC (utility-based collapsing bound model, 22445) < DC (dynamic drift rate collapsing bound model, 22456) < DF (dynamic drift rate fixed bound model, 22628) < SF (static drift rate fixed bound model, 22647). Opinions differ on appropriate thresholds for AIC-based model selection, but the most stringent guidelines suggest that an AIC difference of 14 indicates "very strong support" (Murtaugh, 2014). Therefore, it can be concluded that there is a very strong preference for the collapsing boundary over the fixed boundary (DC vs DF, ΔAIC = 172), and a very strong preference for the dynamic drift rate over the static drift rate (DF vs SF, ΔAIC = 19). The preference for the utility-based model over the perception-based model is not as decisive (UC vs DC, ΔAIC = 11). While this AIC difference can be taken to provide relatively strong support in favor of UC over DC, it does not meet the most stringent thresholds for rejecting DC.

Figure 6 depicts the overall model performance across all participants, and the model fitting results for each participant are shown in the **Appendix Fig. A1 & A2**. The models only make predictions of response time for cross-before trials. The upper panel shows the probability of go decisions and response times. All four models could accurately simulate the probability of go decisions. However, for response times, the fixed boundary models (i.e., DF and SF) performed relatively poorly, failing to capture the increase of response times with increasing TTA conditions. In contrast, the collapsing boundary models successfully captured this pattern, with the UC model showing a slight performance advantage over the DC model. The panel (b) of **Fig. 6** shows the cumulative probability density distribution of response times for cross-before trials, further supporting the above findings. The fitting results of the UC and DC models more closely resemble the experimental data, especially when TTA is 2.5 s and 3 s, compared to the DF

1 and SF models. Additionally, the UC model slightly outperforms the DC model in the upper tail of the
2 response time distribution when TTA is 4 s.
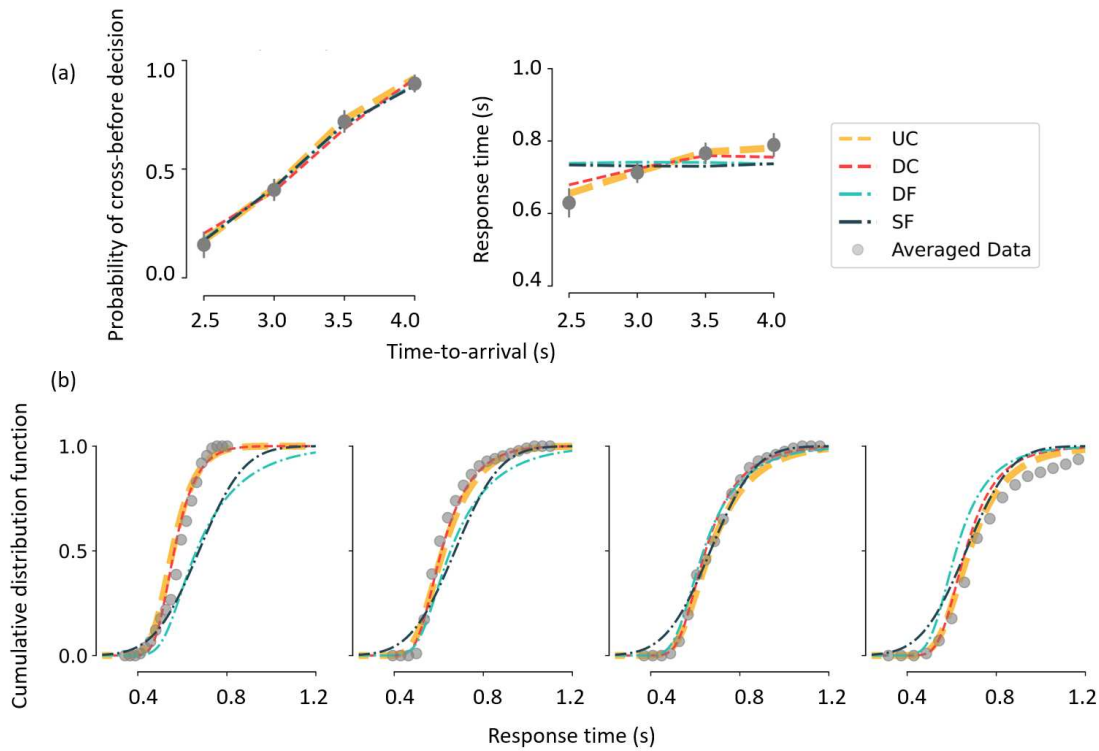
3
4 Fig. 6 Model prediction results. UC: utility-based collapsing bound model, DC: dynamic drift rate collapsing bound
5 model, DF: dynamic drift rate fixed bound model, SF: static drift rate fixed bound model. (a) Group-averaged probability
6 of go decision for all trials, and response time for cross-before trials; (b) probability density function of response time
7 for cross-before trials. The lines represent the model value fitted to the group-averaged data, while the markers represent
8 the group-averaged experimental data.
9

10 3.3 Correlation between accumulated evidence and CPP

11   Based on the findings outlined in Section 3.2, where the UC and DC models demonstrated superior
12 performance compared to other models, this section exclusively focuses on these two models to analyze
13 the correlation between accumulated evidence and CPP. The analysis begins with a qualitative comparison
14 between the two, followed by a quantitative correlation analysis.
15   (1) Qualitative analysis
16   The average stimulus-locked evidence of cross-before and cross-after trials for the DC and UC
17 models are shown in **Fig. 7**. These averages were obtained by generating a simulated dataset of the same
18 size as the original experiment, using the per-participant fitted models, and then averaging the obtained
19 simulated evidence traces across all participants. It can be noted that these average evidence traces appear
20 smoother at the beginning and noisier towards the end. This is because beyond the time point when
21 participants have made decisions, the model evidence is undefined, so the average is across fewer trials.

For cross-before decisions, the average evidence for both the DC and UC models consistently increases toward the upper decision boundary across all TTA conditions. In contrast, for cross-after decisions, the trend of average evidence traces differs between DC and UC models: In the UC model, the average evidence consistently decreases toward the lower decision boundary, in all TTA conditions, whereas in the DC model there is an initial increase and positive evidence peak in the low TTA conditions (2.5 s and 3 s) but not in the high TTA conditions (3.5 s and 4 s). In the cross-after CPP traces in **Fig. 4**, there are no indications of any such qualitative difference in the CPP buildup between the low and high TTA conditions. Instead, the CPP amplitude for cross-after decisions exhibits a continuous increase and peaks around the response time in all TTA conditions, which is qualitatively more similar to the evidence traces for the UC model.

Fig. 8 shows the response-locked evidence traces of DC and UC models, only for trials with cross-before decisions. In the DC model, the accumulated evidence values at response follow a consistent pattern: highest for a TTA of 4 s, followed by 3.5 s, 3 s, and shortest for 2.5 s. In the UC model, the evidence values at the response time are similar at TTAs of 3.5 s and 4 s, both of which are higher compared to the evidence values at TTAs of 2.5 s and 3 s. The evidence value of UC model at response time closely corresponds to the CPP amplitude at the same response time, as shown in **Fig. 5**, where the CPP amplitudes at TTAs of 3.5 s and 4 s are higher than at TTAs of 2.5 s and 3 s.
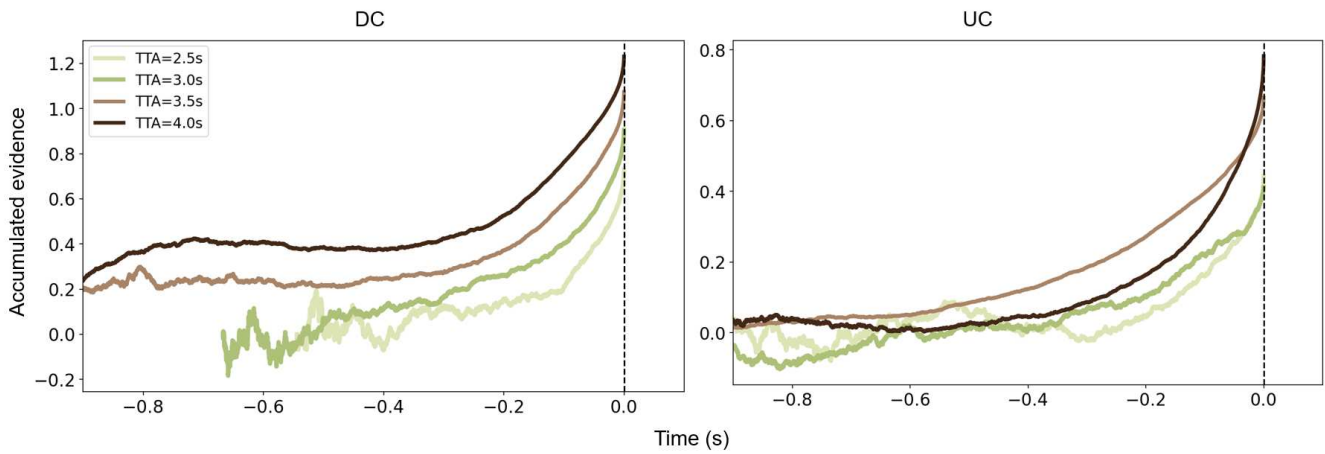
The above qualitative analyses tentatively suggest an alignment between CPP and model evidence that is closer for the UC model than for the DC model, both with stimulus-locked and response-locked signals.
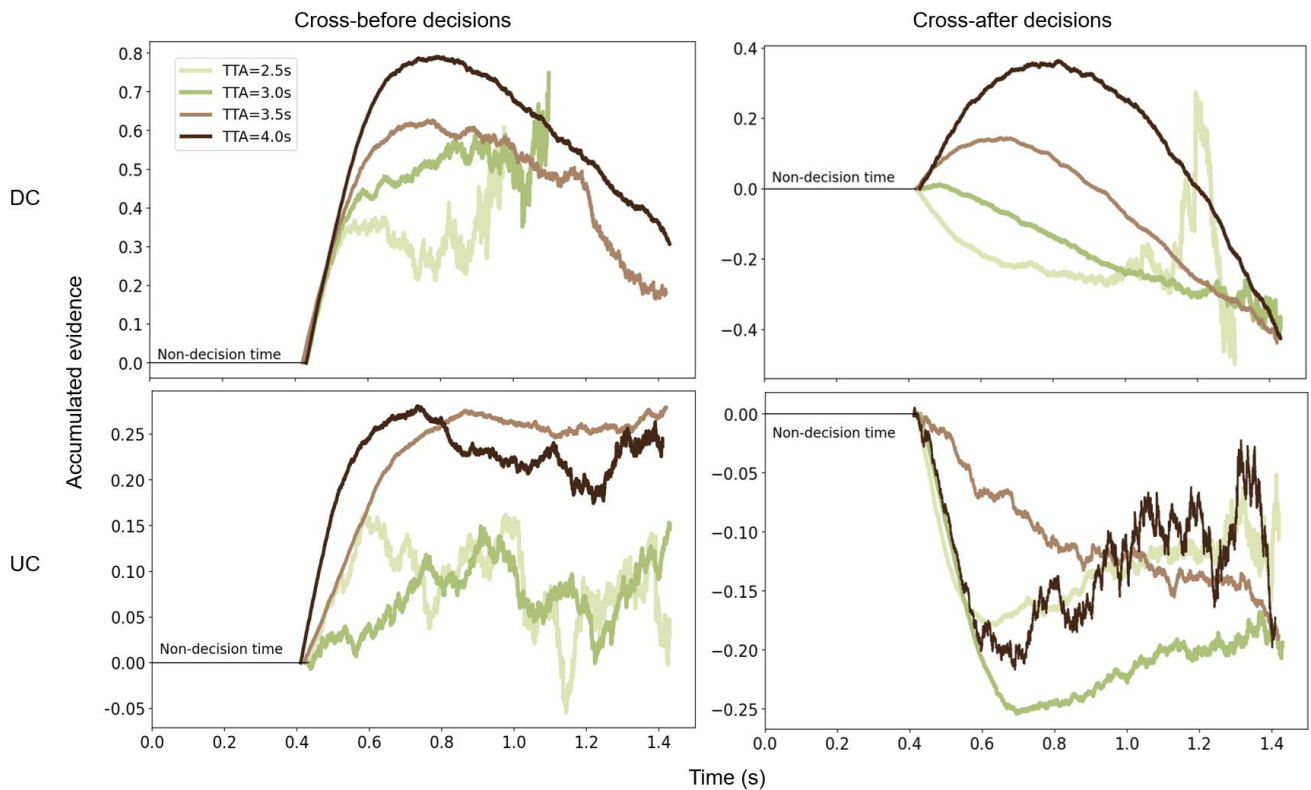
Fig. 7 Comparison of accumulated evidence traces for DC and UC models with cross-before and cross-after decisions.
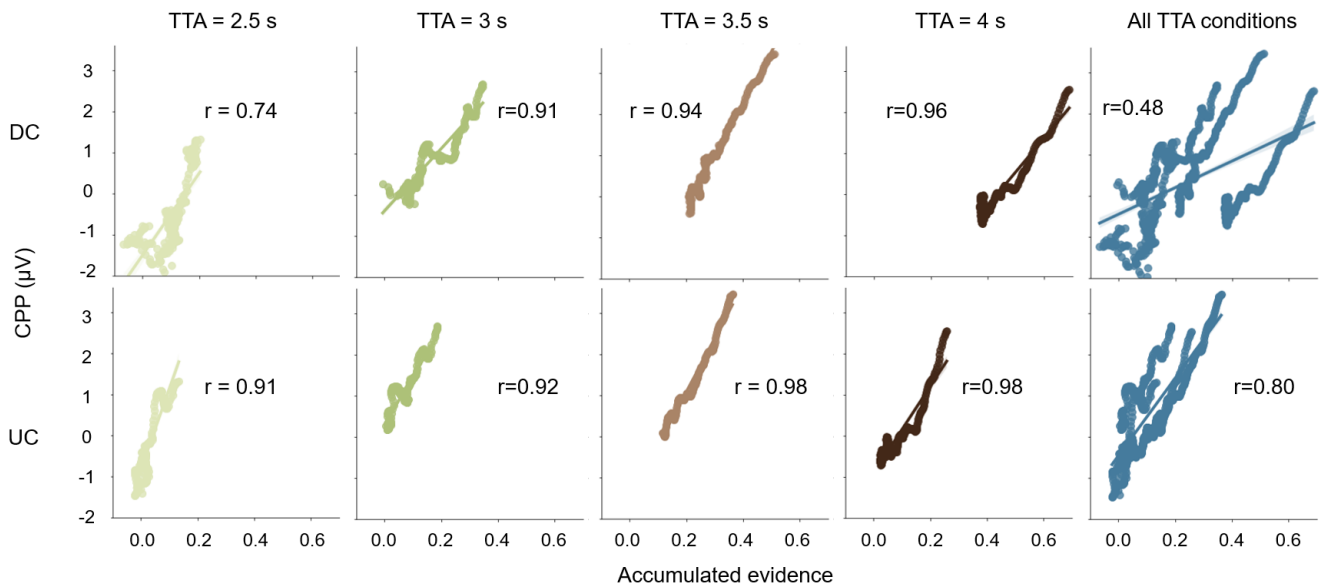

Fig. 8 Response-locked accumulated evidence of cross-before decisions.

(2) Quantitative analysis

Correlation analysis between response-locked CPP amplitude (**Fig. 5**) and response-locked accumulated evidence (**Fig. 8**) was done for the cross-before trials. A time period of 400 ms pre response was chosen since it reflects the typical CPP buildup period in our data (**Fig. 5**).

Fig. 9 show that the CPP amplitude was positively correlated with the evidence in both the DC and UC models across all TTA conditions, with all correlations being statistically significant ($p < 0.01$). The Pearson correlation coefficients show that the coefficients for the UC model is higher than for the DC model in each individual TTA condition, suggesting the evidence buildup in the UC model is more consistent with the observed CPP data. Furthermore, under the assumption that the CPP is a neural correlate of accumulated evidence, we would expect a certain amount of model evidence to correspond to the same CPP amplitude across all conditions. As can also be seen in the rightmost panels of **Fig. 9**, model UC shows this type of consistency across conditions, but not the DC model. This result further strengthens the argument that the UC model generates evidence traces that are more consistent with CPP amplitudes.

Fig. 9 Correlation between response-locked CPP amplitude and response-locked accumulated evidence of the DC and UC models for cross-before trials. r represents correlation coefficient, and all correlations are statistically significant (p < 0.01).

4 Discussion

4.1 An observable CPP signature in the pedestrian crossing task

This study extends the CPP analysis from simple abstract stimuli to a pedestrian crossing scenario, which differs from previous studies of CPP by involving more embodied decision-making about navigating one's own body in the world (albeit virtually). To successfully complete the task, participants needed to track and interpret the movement of the approaching car, and decide when it was safe to cross, balancing their desire to complete the task early against the need to avoid a collision. If the pedestrian intended to cross before the vehicle, they had to make timely decisions based on changing visual cues while respecting time constraints, i.e., the time left for the car to pass. If the pedestrian decided to cross after the vehicle, they had to wait until the car had passed and then initiate their crossing. This set of characteristics of our task sets it clearly apart from previous tasks where a CPP has been observed, such as random dot direction discrimination tasks (Kelly and O'Connell, 2013), and emotion decision task with face morphing (Yau et al., 2021), where participants only need to react to task itself without navigating their own body.

It is notable, then, that despite these differences in task nature, we observed the same type of CPP signature as in the existing literature, with an amplitude buildup leading up to and peaking at response time (Kelly & O'Connell, 2013; Kohl et al., 2020). Furthermore, we found a significant positive correlation between CPP amplitude and accumulated evidence value in DDMs for this applied task, which is in line with previous findings (O'Connell et al., 2018; Van Vugt et al., 2019; Yau et al., 2021). These

findings reinforce the notion of the CPP as a marker for decision-making processes that is remarkably stable across different task contexts and modalities.

In the context of road users, evidence accumulation has long been suggested to play a role, and has been included in models of road user decision-making (Markkula, 2014; Ratcliff and Strayer, 2014; Svärd et al., 2021) and other forms of sustained sensorimotor control (Markkula et al., 2018). Previously, a CPP signature was observed in a task where participants detected collision threats in the form of visual looming from a lead car stimulus (Markkula et al., 2021), but our study is the first to demonstrate this neurophysiological marker of evidence accumulation in a task where the participants make a decision on their own movement. These findings have broad implications for the applicability of CPP measurements in real-world decision-making scenarios. For example, if we extend CPP analysis to domains such as aviation (Čokorilo, 2013), and human-computer interaction (Van Mierlo et al., 2017), we can gain a clearer understanding of how decisions are made under various conditions. This could drive the creation of more effective monitoring tools and the design of more intuitive interfaces, ultimately enhancing both the efficiency and safety of decision-making processes in complex, high-stakes environments.

On the other hand, we found that CPP peak is of a different amplitude for different TTA conditions, which is in line with findings in the random dot motion task (Kohl et al., 2020), abstract gradual target detection task (O'Connell et al., 2012), and human collision threat detection task (Markkula et al., 2018). According to the 'two-accumulator' hypothesis proposed by Markkula et al. (2021), the differing peak amplitudes at response might be attributed to continued evidence accumulation beyond the decision point. This is due to the motor execution delay between reaching the decision threshold and the observable response. In conditions where evidence is more salient, this accumulation process is prolonged, leading to higher peak amplitudes at the time of response.

4.2 DDM performance in the applied pedestrian crossing task

From a modeling perspective, this study found that models with collapsing boundaries showed better fit to the experimental data compared to those with fixed boundaries. These models produced response time distributions that are less skewed, consistent with findings from previous studies (Hawkins et al., 2015; Palestro et al., 2018). However, it should be noted that not all tasks benefit from models with collapsing boundary. Previous studies show that the collapsing boundary is prominent in situations where responses must be made within a strict deadline (Frazier & Yu, 2007; Malhotra, G. et al., 2018; O'Connell et al., 2018). In the pedestrian crossing scenario, as the car approaches, the window of opportunity for the pedestrian to safely cross diminishes rapidly. Therefore, the time when the car approached could be viewed as a strict deadline for decision-making, imposing time pressure on the pedestrian to make a quick decision. This contributes to the observed preference for the collapsing boundary in the DDM model.

Importantly, incorporating the CPP signature into our analysis distinguished between the utility-based model and perception-based model in a way that behavioral data alone could not. Based solely on behavioral data, there was a preference for the utility-based model over perception-based models, but not

to the most stringent requirements of model comparison significance. However, when extending the model comparison to the CPP data, the results showed that the accumulated evidence values in the utility-based model were more closely aligned with the observed CPP amplitude before and at response time, suggesting that this model provides a more accurate representation of the underlying decision process in neural terms. Taken together, these results from both behavioral modeling and model-neurophysiology correlation provide rather compelling evidence in favor of the utility-based account of pedestrian crossing decisions.

The perception-based and utility-based models are based on two different underlying assumptions about how humans achieve locomotion and perceptual-motor control, more broadly. The perceptual account suggests that locomotor decisions are made based on perceptual heuristics, based on information more or less directly available from the perceptual input, in line with ecological psychology theories of human behavior (Gibson, 1958; Fajen 2013; Prédhumeau et al., 2022). In contrast, the utility-based account suggests that locomotor decisions are instead made by estimating the utility, or future rewards, that will come from a decision under consideration. This view of humans as reward-maximisers is also very well-established and actively used, not least in models of locomotion (von Neumann et al., 1944; Hoogendoorn & Bovy, 2003; Markkula et al., 2023).

Looking more specifically at the differences in mathematical assumptions between the DC and UC models, it is not trivial to say exactly what is behind the better performance for the UC model in this case. Behaviorally, the main difference lies in a slightly better capability of the UC model to capture the upper tail of crossing decision times in the 4 s TTA condition (**Fig. 5**). Neurophysiologically, the key reason for the stronger correlation of the UC model evidence with the CPP signal (**Fig. 8**) is that the DC model has a faster evidence buildup early in the trial. Both of these observations may be related to how the two models consider collision risk: The DC model's evidence increment dx is linear around the critical TTA θ_{crit} (Eq. 1), whereas in the UC model, the inverse of TTA in $C(t')$ (Eq. 5) introduces a nonlinearity whereby a change in TTA makes a much bigger difference if TTA is small. At the same time, it should also be pointed out that the theoretical perspectives behind these two models are not strictly incompatible; it may be that humans use perceptual heuristics, but precisely those heuristics which maximize utility. In this vein, one could surely formulate a perceptually available heuristic which approximates well the UC dx in Eq. 5.

One benefit of the utility-based formulation is that it seems easier to generalize to a more diverse set of scenarios. The task of getting to one's goal without colliding with others can be succinctly formulated in terms of a utility or reward function, but the perceptual heuristics required to achieve those rewards may differ substantially between different situations. From this perspective, our favorable results for the utility-based model have applied importance also in the sense that they provide support for this more easily generalizable approach to pedestrian modelling, with applications in traffic safety and vehicle automation (Sadigh et al., 2018; Schwarting et al., 2019; Lin et al., 2022).

4.3 Limitations and future work

There are some limitations in this study. Firstly, the differences between the UC and DC models were quite small, especially behaviorally. Future experiments could be designed in such a way to more clearly separate the two models behaviorally. Secondly, the utility formulation in the UC model tested here is relatively simplistic. In more advanced models of value-based evidence accumulation in simple laboratory tasks, it has been proposed that humans balance the utility of committing to a decision versus the utility of gathering more information (Drugowitsch et al., 2012). In this type of formulation, the estimated utility of gathering more information is highly non-trivial to write analytically, yet it seems reasonable that such processes are also at play in embodied decisions such as pedestrian road-crossing.

5 Conclusion

This study expands the analysis of CPP and DDM from abstract stimuli to an applied pedestrian crossing scenario. The results revealed a typical CPP signature, characterized by a buildup that peaks at response time. Relying solely on behavioral data, there was a partial preference for the utility-based model over perception-based models, while the CPP signature provided additional support for the utility-based model over the perception-based ones in predicting pedestrian road crossing behavior. Since the utility-based model is easier to generalize to a wider range of scenarios, it holds great promise for applications in transport safety and vehicle automation.

Acknowledgments

Data availability

All data are available at https://osf.io/sf7bc/.

References

Bogacz, R., Brown, E., Moehlis, J., Holmes, P., & Cohen, J. D. (2006). The physics of optimal decision making: a formal analysis of models of performance in two-alternative forced-choice tasks. Psychological review, 113(4), 700.

Boyle, N. B., Dye, L., Lawton, C. L., & Billington, J. (2022). A combination of green tea, rhodiola, magnesium, and B vitamins increases electroencephalogram theta activity during attentional task performance under conditions of induced social stress. Frontiers in nutrition, 9, 935001.

Brown, S. D., & Heathcote, A. (2008). The simplest complete model of choice response time: Linear ballistic accumulation. Cognitive psychology, 57(3), 153-178.

Busemeyer, J. R., & Townsend, J. T. (1993). Decision field theory: a dynamic-cognitive approach to decision making in an uncertain environment. Psychological review, 100(3), 432.

Camara, F., Bellotto, N., Cosar, S., Weber, F., Nathanael, D., Althoff, M., Wu, J., Ruenz, J., Dietrich, A., Markkula, G., Schieben, A., Tango, F., Merat, N., & Fox, C. (2020). Pedestrian models for autonomous driving part II: High-level models of human behavior. IEEE Transactions on Intelligent Transportation Systems pp. 120.https://doi.org/10.1109/TITS.2020.3006767 .

Čokorilo, O. (2013). Human factor modelling for fast‐time simulations in aviation. Aircraft Engineering and Aerospace Technology, 85(5), 389-405.

Delorme, A., & Makeig, S. (2004). EEGLAB: an open source toolbox for analysis of single-trial EEG dynamics including independent component analysis. Journal of neuroscience methods, 134(1), 9-21.

Delorme, A., Sejnowski, T., & Makeig, S. (2007). Enhanced detection of artifacts in EEG data using higher-order statistics and independent component analysis. Neuroimage, 34(4), 1443-1449.

Drugowitsch, J., Moreno-Bote, R., Churchland, A. K., Shadlen, M. N., & Pouget, A. (2012). The cost of accumulating evidence in perceptual decision making. Journal of Neuroscience, 32(11), 3612-3628.

Fajen, B. R. (2013). Guiding locomotion in complex, dynamic environments. Frontiers in Behavioral Neuroscience, 7. https://doi.org/10.3389/fnbeh.2013.00085

Fitzpatrick, K., Turner, S., Brewer, M., Carlson, P., Ullman, B., Trout, N., Park, E. S., Whitacre, J., Lalani, N., & Lord, D. (2006). Improving pedestrian safety at unsignalized crossings. National Academy Press.

Forstmann, B. U., & Wagenmakers, E. J. (2014). An introduction to model-based cognitive neuroscience. New York, NY: Springer

Forstmann, B. U., Anwander, A., Schäfer, A., Neumann, J., Brown, S., Wagenmakers, E. J., ... & Turner, R. (2010). Cortico-striatal connections predict control over speed and accuracy in perceptual decision making. Proceedings of the National Academy of Sciences, 107(36), 15916-15920.

Forstmann, B. U., Wagenmakers, E. J., Eichele, T., Brown, S., & Serences, J. T. (2011). Reciprocal relations between cognitive neuroscience and formal cognitive models: opposites attract?. Trends in cognitive sciences, 15(6), 272-279.

Frazier, P., & Yu, A. J. (2007). Sequential hypothesis testing under stochastic deadlines. Advances in neural information processing systems, 20.

Gibson, J. J. (1958). Visually controlled locomotion and visual orientation in animals. British Journal of Psychology, 49(3), 182–194. https://doi.org/10.1111/j.2044-8295.1958.tb00656.x

González-Méndez, M., Olaya, C., Fasolino, I., Grimaldi, M., & Obregón, N. (2021). Agent-based modeling for urban development planning based on human needs. Conceptual basis and model formulation. Land Use Policy, 101, 105110.

Hawkins, G. E., Forstmann, B. U., Wagenmakers, E. J., Ratcliff, R., & Brown, S. D. (2015). Revisiting the evidence for collapsing boundaries and urgency signals in perceptual decision-making. Journal of Neuroscience, 35(6), 2476-2484.

Hoogendoorn, S., & Bovy, P. H. L. (2003). Simulation of pedestrian flows by optimal control and differential games. Optimal Control Applications and Methods, 24(3), 153–172. https://doi.org/10.1002/oca.727

Kelly, S. P., & O'Connell, R. G. (2013). Internal and external influences on the rate of sensory evidence accumulation in the human brain. Journal of Neuroscience, 33(50), 19434-19441.

Kohl, S. H., Mehler, D. M., Lührs, M., Thibault, R. T., Konrad, K., & Sorger, B. (2020). The potential of functional near-infrared spectroscopy-based neurofeedback—a systematic review and recommendations for best practice. Frontiers in neuroscience, 14, 594.

Lin, Y. S., Srinivasan, A. R., Leonetti, M., Billington, J., & Markkula, G. (2022). A utility maximization model of pedestrian and driver interactions. IEEE Access, 10, 118888-118899.

Malhotra, G., Leslie, D. S., Ludwig, C. J., & Bogacz, R. (2018). Time-varying decision boundaries: insights from optimality analysis. Psychonomic bulletin & review, 25, 971-996.

Markkula, G. (2014). Modeling driver control behavior in both routine and near-accident driving. Proceedings of the Human Factors and Ergonomics Society Annual Meeting, 58(1), 879–883. https://doi.org/10.1177/1541931214581185

Markkula, G., Boer, E., Romano, R., & Merat, N. (2018). Sustained sensorimotor control as intermittent decisions about prediction errors: Computational framework and application to ground vehicle steering. Biological Cybernetics, 112(3), 181–207. https://doi.org/10.1007/s00422-017-0743-9

Markkula, G., Madigan, R., Nathanael, D., Portouli, E., Lee, Y. M., Dietrich, A., … Merat, N. (2020). Defining interactions: a conceptual framework for understanding interactive behaviour in human and automated road traffic. Theoretical Issues in Ergonomics Science, 21(6), 728–752. https://doi.org/10.1080/1463922X.2020.1736686

Markkula, G., Lin, Y. S., Srinivasan, A. R., Billington, J., Leonetti, M., Kalantari, A. H., ... & Merat, N. (2023). Explaining human interactions on the road by large-scale integration of computational psychological theory. PNAS nexus, 2(6), pgad163.

Markkula, G., Uludağ, Z., Wilkie, R. M., & Billington, J. (2021). Accumulation of continuously time-varying sensory evidence constrains neural and behavioral responses in human collision threat detection. PLoS Computational Biology, 17(7), e1009096.

McGovern, D. P., Hayes, A., Kelly, S. P., & O'Connell, R. G. (2018). Reconciling age-related changes in behavioural and neural indices of human perceptual decision-making. Nature human behaviour, 2(12), 955-966.

Murtaugh, P. A. (2014). In defense of P values. Ecology, 95(3), 611–617. https://doi.org/10.1890/13-0590.1

Nolan H, Whelan R, Reilly RB. FASTER: fully automated statistical thresholding for EEG artifact rejection. J Neurosci Methods. (2010) 192:15262. doi: 10.1016/j.jneumeth.2010.07.015

Nunez, M. D., Vandekerckhove, J., & Srinivasan, R. (2017). How attention influences perceptual decision making: Single-trial EEG correlates of drift-diffusion model parameters. Journal of mathematical psychology, 76, 117-130.

O'Connell, R. G., Dockree, P. M., & Kelly, S. P. (2012). A supramodal accumulation-to-bound signal that determines perceptual decisions in humans. Nature neuroscience, 15(12), 1729-1735.

Oostenveld, R., Fries, P., Maris, E., & Schoffelen, J. M. (2011). FieldTrip: open source software for advanced analysis of MEG, EEG, and invasive electrophysiological data. Computational intelligence and neuroscience, 2011(1), 156869.

Palestro, J. J., Bahg, G., Sederberg, P. B., Lu, Z. L., Steyvers, M., & Turner, B. M. (2018). A tutorial on joint models of neural and behavioral measures of cognition. Journal of Mathematical Psychology, 84, 20-48.

Parker, S., & Ramsey, R. (2024). What can evidence accumulation modelling tell us about human social cognition?. Quarterly Journal of Experimental Psychology, 77(3), 639-655.

Pekkanen, J., Giles, O. T., Lee, Y. M., Madigan, R., Daimon, T., Merat, N., & Markkula, G. (2022). Variable-drift diffusion models of pedestrian road-crossing decisions. Computational Brain & Behavior, 1-21.

Petzoldt, T. (2014). On the relationship between pedestrian gap acceptance and time to arrival estimates. Accident Analysis & Prevention, 72, 127-133.

Prédhumeau, M., Mancheva, L., Dugdale, J., & Spalanzani, A. (2022). Agent-Based Modeling for Predicting Pedestrian Trajectories Around an Autonomous Vehicle. Journal of Artificial Intelligence Research, 73, 1385–1433. https://doi.org/10.1613/jair.1.13425

Purcell, B. A., Heitz, R. P., Cohen, J. Y., Schall, J. D., Logan, G. D., & Palmeri, T. J. (2010). Neurally constrained modeling of perceptual decision making. Psychological review, 117(4), 1113.

Ratcliff, R. (1978). A theory of memory retrieval. Psychological review, 85(2), 59.

Ratcliff, R., & McKoon, G. (2008). The diffusion decision model: theory and data for two-choice decision tasks. Neural computation, 20(4), 873-922.

Ratcliff, R., & Rouder, J. N. (1998). Modeling response times for two-choice decisions. Psychological science, 9(5), 347-356.

Ratcliff, R., & Strayer, D. (2014). Modeling simple driving tasks with a one-boundary diffusion model. Psychonomic Bulletin & Review, 21(3), 577–589. https://doi.org/10.3758/s13423-013-0541-x

Ratcliff, R., & Tuerlinckx, F. (2002). Estimating parameters of the diffusion model: Approaches to dealing with contaminant reaction times and parameter variability. Psychonomic bulletin & review, 9(3), 438-481.

Ricciardi, L. M. (1976). On the transformation of diffusion processes into the Wiener process. Journal of Mathematical Analysis and Applications, 54(1), 185-199.

Sadigh, D., Landolfi,N.,Sastry,S.S.,Seshia,S.A.,&Dragan,A.D. (2018). Planning for cars that coordinate with people: Leveraging effects on human actions for planning and active information gathering over human internal state. Autonomous Robots, 42(7), 1405–1426. https://doi.org/10.1007/s10514-018-9746-1

Schiff, W., & Oldak, R. (1990). Accuracy of judging time to arrival: Effects of modality, trajectory, and gender. Journal of Experimental Psychology. Human Perception and Performance, 16(2), 303–316. https://doi.org/10.1037//0096-1523.16.2.303

Schwarting, W., Pierson, A., Alonso-Mora, J., Karaman, S., & Rus, D. (2019). Social behavior for autonomous vehicles. Proceedings of the National Academy of Sciences, 116(50), 201820676. https://doi.org/10.1073/pnas.1820676116

Shinn, M., Lam, N. H., & Murray, J. D. (2020). A flexible framework for simulating and fitting generalized drift-diffusion models. ELife, 9, e56938.

Steinemann, N. A., O'Connell, R. G., & Kelly, S. P. (2018). Decisions are expedited through multiple neural adjustments spanning the sensorimotor hierarchy. Nature communications, 9(1), 3627.

Sutton, S., Braren, M., Zubin, J., & John, E.R. (1965). Evoked-Potential Correlates of Stimulus Uncertainty. Science, 150, 1187 - 1188.

Svärd, M., Markkula, G., Bärgman, J., & Victor, T. (2021). Computational modeling of driver pre-crash brake response, with and without off-road glances: Parameterization using real-world crashes and near-crashes. Accident Analysis & Prevention, 163, 106433. https://doi.org/10.1016/j.aap.2021.106433

Tagliabue, C.F., Veniero, D., Benwell, C.S., Cecere, R., Savazzi, S., & Thut, G. (2019). The EEG signature of sensory evidence accumulation during decision formation closely tracks subjective perceptual experience. Scientific Reports, 9.

Tajima, S., Drugowitsch, J., & Pouget, A. (2016). Optimal policy for value-based decision-making. Nature communications, 7(1), 12400.

Theisen, M., Schießl, C., Einhäuser, W., & Markkula, G. (2024). Pedestrians' road-crossing decisions: Comparing different drift-diffusion models. International Journal of Human-Computer Studies, 183, 103200.

Turner, B. M., Van Maanen, L., & Forstmann, B. U. (2015). Informing cognitive abstractions through neuroimaging: the neural drift diffusion model. Psychological review, 122(2), 312.

UCSD Swartz Center for Computational Neuroscience (2022). Makoto's preprocessing pipeline. Retrieved from https://sccn.ucsd.edu/wiki/Makoto's_preprocessing_pipeline

Van Mierlo, S., Van Tendeloo, Y., Meyers, B., & Vangheluwe, H. (2017). Domain-specific modelling for human–computer interaction. The Handbook of Formal Methods in Human-Computer Interaction, 435-463.

van Vugt, M. K., Beulen, M. A., & Taatgen, N. A. (2019). Relation between centro-parietal positivity and diffusion model parameters in both perceptual and memory-based decision making. Brain research, 1715, 1-12.

von Neumann, J., Morgenstern, O., & Rubinstein, A. (1944). Theory of Games and Economic Behavior. Princeton University Press. https://www.jstor.org/stable/j.ctt1r2gkx

Wang, T., Ge, Y. E., Wang, Y., Chen, W., Fu, Q., & Niu, Y. (2024). A novel model for real-time risk evaluation of vehicle–pedestrian interactions at intersections. Accident Analysis & Prevention, 206, 107727.

Yau, Y., Hinault, T., Taylor, M., Cisek, P., Fellows, L. K., & Dagher, A. (2021). Evidence and urgency related EEG signals during dynamic decision-making in humans. Journal of Neuroscience, 41(26), 5711-5722.
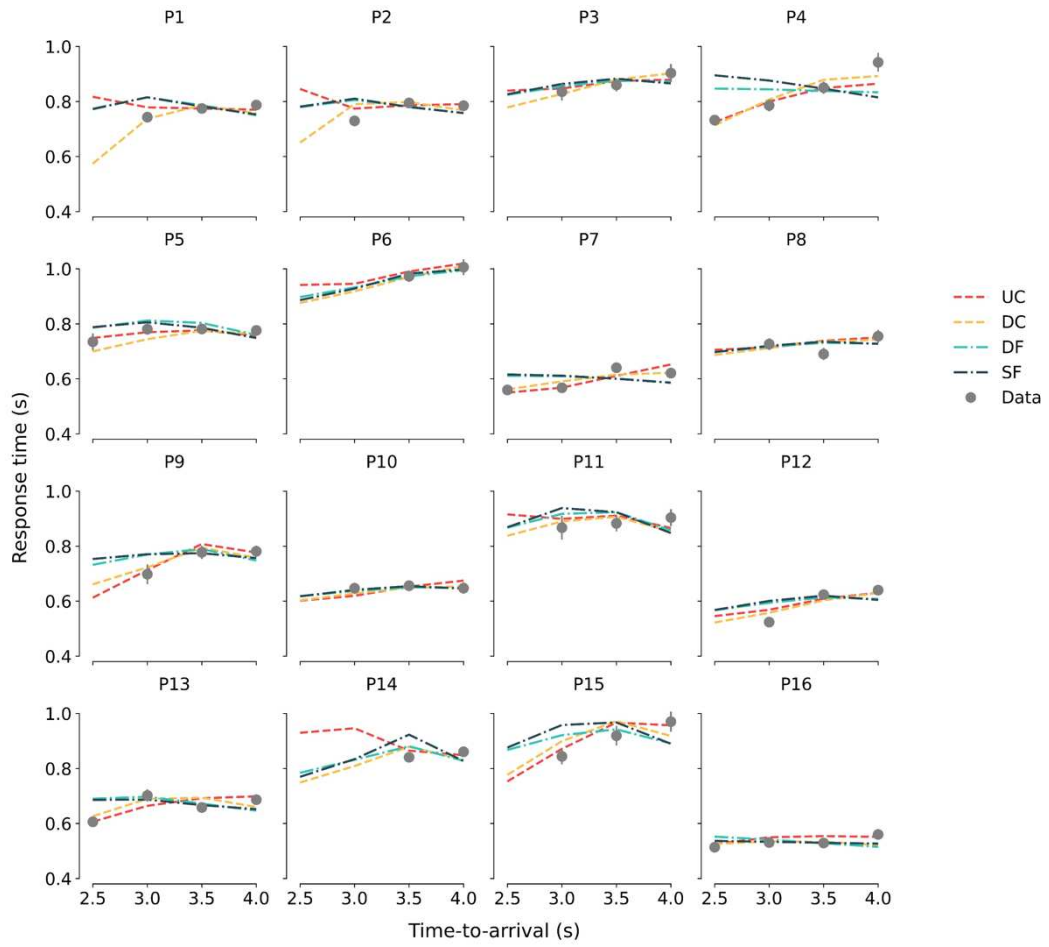
Zgonnikov, A., Abbink, D., & Markkula, G. (2024). Should I stay or should I go? Cognitive modeling of left-turn gap acceptance decisions in human drivers. Human factors, 66(5), 1399-1413.

Appendix
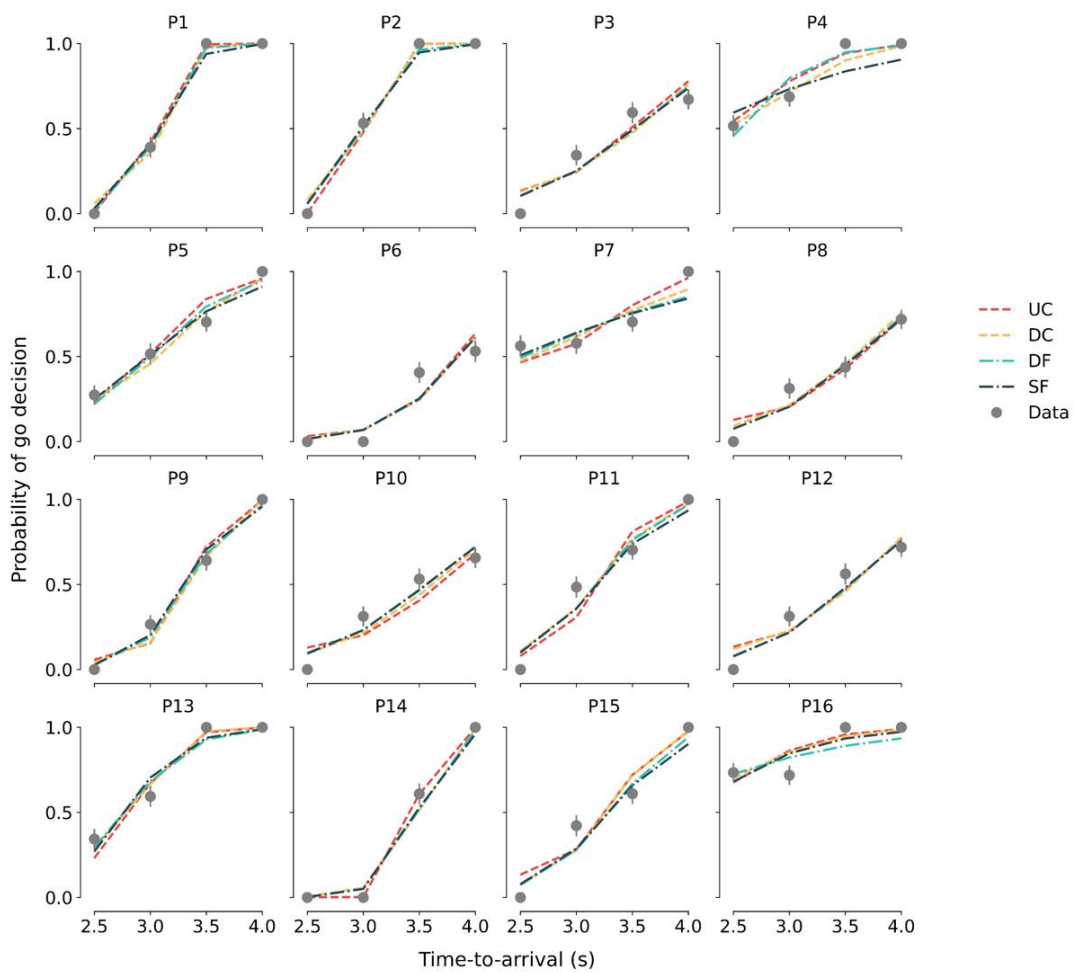
Fig. A1 Probability of cross-before decision for four models fitted to experimental data. Error bars indicate binomial proportion standard error of mean.

1

Fig. A2 Response time of cross-before decision for four models fitted to experimental data. Response times for conditions with less than 15 data points are omitted. Error bars indicate standard error of mean.